IEEE Access
Multidisciplinary | Rapid Review | Open Access Journal

Received 3 November 2022, accepted 22 November 2022, date of publication 30 November 2022,
date of current version 5 December 2022.

Digital Object Identifier 10.1109/ACCESS.2022.3225522

APPLIED RESEARCH

A Novel Nonlinear Plus Integral Controller With a Real-Time Application on Incubator Temperature Regulation

M. ONAT, (Member, IEEE)
Department of Electrical and Electronics Engineering, Faculty of Engineering, Marmara University, 34854 Istanbul, Turkey
e-mail: monat@marmara.edu.tr

ABSTRACT A gel card incubator is a significant clinical interface device that brings the gel card's temperature up, and maintains it at body temperature, and completes the initial step in determining the blood grouping. Achieving a much faster closed-loop response to shorten the warm-up period and maintaining a uniform temperature inside the incubator are crucial requirements for medical incubation devices. To accomplish the incubator control requirements and deal with deadtime, this study proposes a novel nonlinear plus integral control (NPI) scheme coupled with a time-delay compensator using an incubator dynamics model. The NPI successfully shaped the control structure by utilizing a few nonlinear parameters. The control strategy, which promises significant performance by combining linear and nonlinear control actions, is easy to realize, simple to tune, and allows smooth transition between control actions. Experiments were performed in a microprocessor-controlled gel card incubator by using a computer interface to demonstrate the superiority of the proposed control technique. The comparative results prove that the proposed control scheme exhibits superior responses for transient and steady states. It also achieves successful disturbance rejection and less energy consumption than the Smith predictor-based proportional integral (PI) control.

INDEX TERMS Body temperature, gel card incubator, nonlinear plus integral controller, Smith predictor, temperature control.

I. INTRODUCTION

Temperature regulation, possibly the most well-known engineering task, is employed in a variety of medical applications, including PCR tests [1], neonatal infant incubators [2], [3], gel card incubators [4], blood banks, patient temperature monitors, and other diagnostic and analytical tools.

One of the basic requirements of biochemistry laboratories is to maintain a constant temperature at predetermined levels during the working hours. For example, the gel-based agglutination test, which is extensively used for blood typing, produces the most accurate results when stabilized at the body temperature [5]. This test is based on the gel technique for detecting red blood cell agglutination reactions, wherein the gel acts as a trap [4]. Therefore, the gel card incubator (hereafter ''incubator'') is a vital intermediate device that brings the temperature of the gel card to the body temperature of $37°C$ before the blood grouping test, which usually takes 10-15 minutes [6].

Incubators exhibit dead-time characteristics such as systems that extend from the process industry [7], [8] to automotive engines [9], [10]. Therefore, shortening the warm-up phase and achieving reliable incubation should rest on a high-performance control scheme. When employing low-performance control strategies such as PI control for a dead-time incubator, the system either sluggishly reaches $37°C$, increasing overall processing time, or oscillates, delaying the system's settling to body temperature. Even if accompanying PI control with the Smith predictor (SP) increases performance, it falls short of the expected efficacy in terms of a short warm-up period, thereby wasting time and energy. Therefore, traditional approaches make it difficult to obtain

The associate editor coordinating the review of this manuscript and approving it for publication was Azwirman Gusrialdi.

a higher control precision. This study aims to achieve reliable incubation with a novel control strategy that adequately reduces the incubator warm-up phase with a faster transient response, achieving tracking control with negligible error, and disturbance rejection with a quick settling time.

With the first effective dead-time compensator pioneered by [11], published in the middle of the previous century, studies [12], [13] on the stability and performance improvement of dead-time systems, particularly those encountered in the industry and engineering fields, have continued. A significant part of the control approaches directly use the SP [12], [13] or improved versions [14], [15], [16]. Other researchers [17] have employed a dead-time compensator to counteract undesirable oscillatory closed-loop responses, instability, and other disturbance effects. On the other hand, as for the gel card incubator, to the author's best knowledge, no work is reported in the literature on SP based temperature regulation. Neonatal infant incubators and their varieties have frequently been discussed. However, they often include traditional control schemes such as bang-bang and PID, which are widely known to perform poorly against plants with dead times [17], [18]. In addition, adaptive predictive control [2] and fuzzylogic control schemes [19] have been developed Zermani et al. proposed an adaptive generalized predictive control utilizing the recursive least squares technique for system nonlinearities, considering parametric uncertainty to improve temperature control performance [2]. In another study, Shaaban et al. employed a fuzzy control strategy to eliminate modeling and tuning problems and achieve accurate temperature regulation [20]. The results are slightly different from those of traditional controllers. However, these control approaches have only been applied to short deadtime systems [20] does not appear appropriate, because fuzzy control alone cannot overcome dead-time problems [21].

Considering the dead-time dynamics of the gel card incubator, a specially tailored nonlinear type controller (NPI) was realized in conjunction with the SP by bringing the temperature to the setpoint faster and tracking it with zero error during the warm-up phase and after insertion of the new gel cards. The control scheme that achieves these goals comprises of three control components. First, the power function with an exponent that provides a high gain over a large error range brings the plant temperature to the setpoint much faster during warm-up. Second, the product of the power and exponential functions acted as a clamp to maintain the temperature around the set point. Because the component (control action) is like a bell-shaped curve symmetrical about the origin, it can effectively provide the required gain to force the tracking error to zero within a parameter-adjusted error range. Third, the integrator function eliminates offset errors with common features.

The study accomplishes the following objectives: a) introducing a novel nonlinear control strategy, b) conducting an experimental implementation to demonstrate the effectiveness and validity of the proposed control strategy, c) providing a much faster response time to shorten the warm-up period, d) maintaining body temperature during the incubation, and e) preventing blood sample deterioration due to overheating (overshoot).

FIGURE 1. The gel card incubator (left) with a gel card (right).

The remainder of this paper is organized as follows. Section II introduces the peripheral units of the gel card incubator, nonlinear control structure, and dead-time compensator-based temperature control system. Section III presents experimental results and a comparative discussion of each control scheme. Finally, the last section provides concluding remarks.

II. GEL CARD INCUBATOR AND CONTROL

The system is a laboratory-scale heating process aimed at testing a novel control strategy, teaching well-known automatic control techniques through the temperature control user interface and incubating gel cards with precision.

A. STRUCTURE AND WORKING PRINCIPLE

The incubator was composed of a rectangular outer metal case with dimensions of 400 mm × 325 mm × 90 mm and an inner metal tank with dimensions of 215 mm × 215 mm × 75 mm. Two-zone metal grids with thin slots were mounted on a rectangular metal tank with a capacity of 24 gel cards and 6-column microtubes, as illustrated in Fig. 1 (right). Gel cards are kept at low temperatures unless incubated. The incubation device comprises 150-W cartridge tubular resistive heating element for dry air, two temperature sensors (LM35) with an accuracy error of $\mp 0.2^{\circ}C$, a microcontroller (ATMega 2560)-based heater SCR drive, and heat insulation materials.

The heater was housed in the tank base, extending between two identical grid blocks, allowing heat to be transferred to all grid surfaces by convection. The first temperature sensor was placed in contact with a gel card on a grid. Because the heater was sufficiently distant from the sensor points, fluctuations in the delay times between the sensor locations could be ignored. The second sensor measures the ambient temperature outside the incubator.

During successive incubation processes, the net heat accumulated in the incubator tank is given by

$$Q_{cham} = Q_{heater} - Q_{loss} - Q_{locex} \tag{1}$$

where Q_{cham} is the net heat accumulated in the tank, Q_{heater} is the heat transfer from the heater to the tank, Q_{loss} is the heat

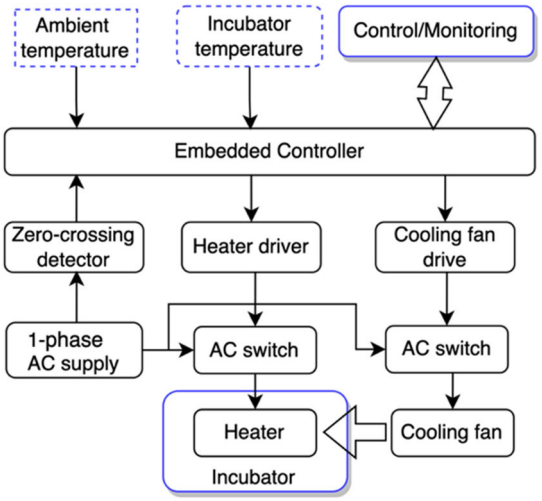

FIGURE 2. Controlling and monitoring structure of the system.

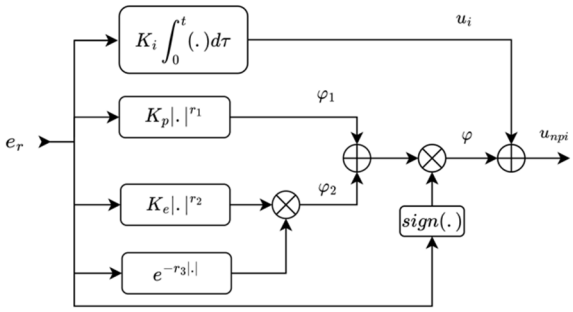

FIGURE 3. NPI control scheme.

transfer from the incubator to the outdoor environment, and Q_{locex} is the heat loss during replacement and heat exchange of the gel cards.

This study assumes a first-order plus dead-time (FOPDT) model because it shows a reasonably good match with a dynamic process. In addition, many studies [22], [23] have considered it sufficient to work with the first-order model.

Fig. 2 shows the schematic of the control and monitoring systems. Apart from the incubator tank, the setup includes heater and cooling (disturbance purpose only) units, and their drives are controlled by an embedded microprocessor circuitry. The monitoring unit, which includes a microcontroller-based audio configurable alarm and a digital display (LED) to set the timer and monitor the incubation, is beyond the scope of this study, as shown in the front console of Fig. 1. The details of the incubator equipment are discussed in Section III.

B. INTRODUCING NONLINEAR CONTROLLER (NPI)

As shown in Fig. 3, the block diagram of the NPI comprises three main components coupled in parallel, as defined by (2), (3), and (4). Dots inside and |.| stand for the error e_r.

$$\varphi_1 = K_p \left|e_r\left(t\right)\right|^{r_1} \tag{2}$$

$$\varphi_2 = K_e \left|e_r\left(t\right)\right|^{r_2} e^{-r_3\left|e_r(t)\right|} \tag{3}$$

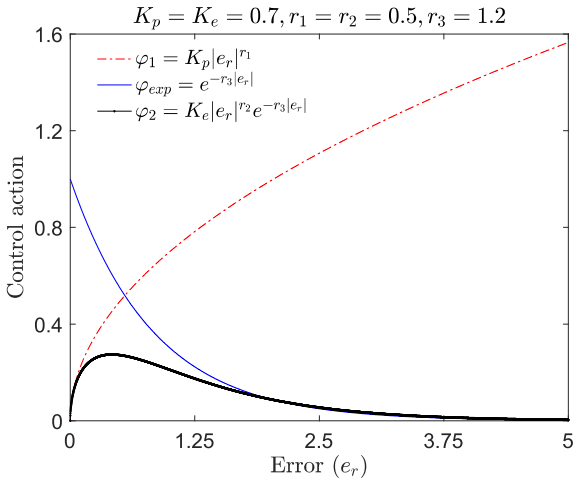

FIGURE 4. Functions constituting nonlinear control components φ_1 *and* φ_2.

$$u_i = K_i \int_0^t e\left(\tau\right) d\tau \tag{4}$$

where r_1, r_2, and r_3 are the positive real values. φ_1 is a power function with a base $|e_r\left(t\right)|$, absolute value of error, and exponent r_1, and φ_2 is the product of the power and exponential functions. The power function can quickly reduce the transient response time when both the r_1 and e_r are higher than one, providing much more gain. The φ_2 can achieve an adjustable gain and slope owing to its bell-shaped (concave up/down) curve characteristics to maintain the tracking error within a small-error region. The last control component u_i in (4) is the integrator, which eliminates steady-state offset errors. The φ is the resultant nonlinear component (5) of φ_1 and φ_2 (coupled in parallel) and multiplied by a sign function representing the sign of the error, $e_r\left(t\right)$.

$$\varphi = sign(e_r\left(t\right))\left(\varphi_1 + \varphi_2\right) \tag{5}$$

The control effort signal u_{npi} in (6) is a parallel-coupled combination of the linear and nonlinear control components.

$$u_{npi}\left(t\right) = \varphi + u_i \tag{6}$$

The power function φ_1 with $r_1 \neq 1$ (dash-dotted red) and the product of the power and exponential (φ_{exp}, solid blue) functions φ_2 (bold solid black) constitute the nonlinear controller components, as shown in Fig. 4. The parameter settings were $K_p = K_e = 0.7$, $r_1 = r_2 = 0.5$, $r_3 = 1.2$, as shown in the figure. The absolute value of the error signal makes φ_1 and φ_2 symmetric to the y axis (even function). Multiplying by a sign function as a control requirement causes the components to be symmetric with respect to the origin (odd function), as illustrated in Fig. 5. The parameters for Fig. 5 were set to $K_p = K_e = 0.15$, $r_1 = r_2 = 0.3$, and $r_3 = 1.2$ to demonstrate nonlinear component actions. Accordingly, the proposed controller can act linearly by setting $r_1 = 1$ and $K_e = 0$ or nonlinearly by selecting r_1 and K_e as positive real values. The gains (K_p, K_e) and exponents (r_1, r_2, r_3) provide individual contributions to the controller construction, as will be discussed later.

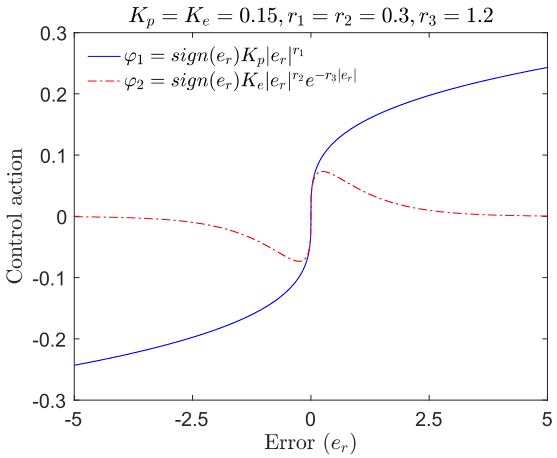

FIGURE 5. Making nonlinear control components symmetrical about the origin.

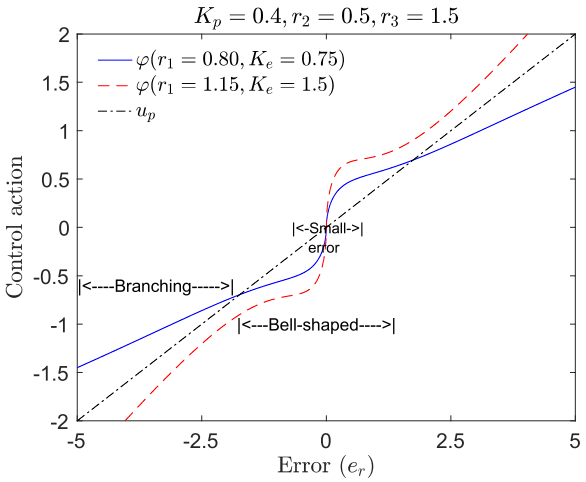

FIGURE 6. Nonlinear control action regions.

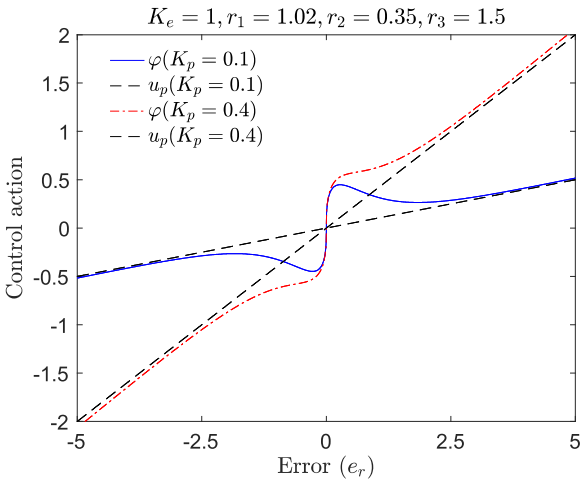

FIGURE 7. Changing slopes of control action curves with K_p.

Fig. 6 shows the typical nonlinear φ control action lines (solid blue and dashed red) and P-control action line (dash-dotted black). The P control action (u_p) is used for comparison with nonlinear control actions to better understand the parameter effects of the nonlinear control components. Note that the parameter values of the control actions used in this section are not experimental but are intended to help better understand their effects through increased graphical visualization.

Because of its nonlinear dynamics, φ can effectively output high gains by increasing K_e at points where small error variations occur, bringing the plant output to the setpoint faster. At higher scaled errors, based on r_1, φ symmetrically branches beyond the bell-shaped region, either cutting the P action line ($u_p = K_p e_r$), exhibiting concave behavior or moving away from the P action line, demonstrating convex behavior, as shown in the figure. Therefore, nonlinear control action can be divided into three regions: branching, small error, and bell shape.

For a plant, a simple tuning guide can be suggested for NPI parameter settings as follows: First, starting with PI control by setting $r_1 = 1$ and $K_e = 0$, the PI control tuning parameters K_p and K_i can be obtained with reasonable initial values using the Zeigler-Nichols method based on the plant model. For parameter tuning of φ_1, r_1 can be set higher than 1, usually up to 1.5, to achieve a faster transient response. For parameter settings of φ_2 in the small-error region, K_e, with a broad setting range of 10–35, can appropriately adjust the gain by altering the bell-shaped curve without changing the slope of the control action. Finally, the r_3, with a range of 0.1 to 1.2, forces the plant output to remain in the small-error region by modifying the concavity/convexity range (size) of the control action without affecting the slope.

C. GENERATING CONTROL ACTIONS WITH TUNING PARAMETERS

This section presents the φ control actions based on the tuning parameters of K_p, K_e, r_1, r_2, and r_3 within the error range of -5 to 5. The shaping of the control signal by the effect of each tuning parameter versus the error is graphically depicted by adjusting only one parameter at a time while leaving the others unchanged.

Fig. 7 illustrates the φ and u_p control actions by selecting the gain K_p as 0.1 and 0.4 with the set parameters in the figure. Note that the K_p rotates the control actions with respect to the origin and modifies the bell-shaped curve without changing the slope.

Fig. 8 shows the φ control actions by choosing K_e as 0.75 and 1.5 with the set parameters. As shown, the K_e modifies the concavity (up and down) of the control-action curve and its gain. The control action curve (bell-shaped) confines the plant's output error within the small-error region. Note that K_e does not affect the slope of the control-action curve.

Setting the power exponent r_1 to 0.85 and 1.2 with the set parameters, is shown in Fig. 9. Like the preceding parameters, r_1 has no influence on the slope in the small-error region. When $r_1 < 1$ is set, the φ branches (solid blue line) deviate from the P action line, as shown

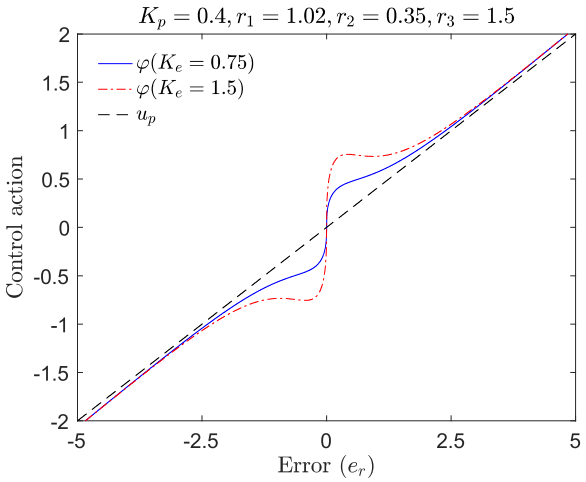

FIGURE 8. Increasing concavity/convexity and gain with increasing K_e.

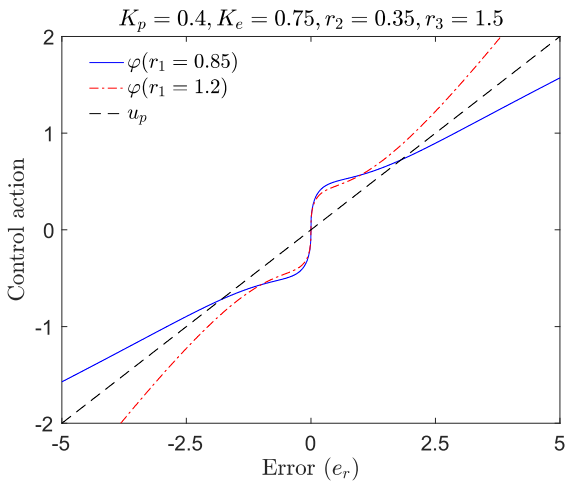

FIGURE 9. Moving away and deviation of ϕ branches.

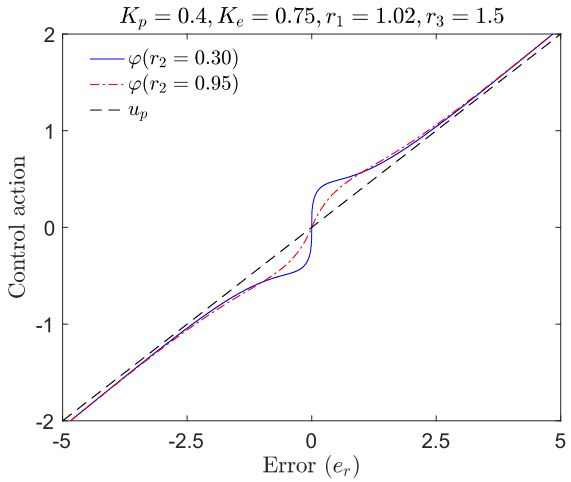

FIGURE 10. Simultaneous variations in slope and bell-shaped curve.

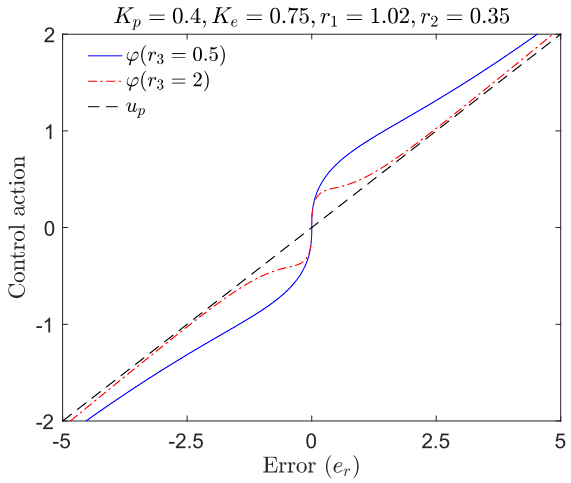

FIGURE 11. Modifying bell-shaped curve range.

in the figure. Setting $r_1 > 1$ causes φ to behave in a convex manner (red line) and move away from the P-action line. In other words, φ action can quickly reduce the error to acceptable levels, taking instability that may occur into account. Furthermore, it can achieve a faster decrease in gain as the error approaches the set point ($r_1 > 1, |e_r(t)| < 1$), thereby contributing to the zero-tracking error.

Setting the exponent r_2 to 0.30 and 0.95 with the set parameters causes simultaneous variations in the slope and bell-shaped curve of φ, as illustrated in Fig. 10. φ changes from sluggish (soft) to fast (hard) as r_2 decreases, thereby increasing the degree of nonlinearity. Thus, the tuning parameter r_2 appears to be dominant in shaping the slope of the control action, ranging from P-control to sliding-mode control.

Fig. 11 illustrates the φ actions by selecting r_3 0.5 and 2.0 with the set parameters. The φ branches move away from the P-action line, and φ behaves as a hyperbolic function as r_3 decreases. Thus, setting r_3 forces the plant output to remain stable in the small-error region by altering the bell-shaped range.

Various control actions can be performed by tuning φ, as illustrated in Fig. 12 and 13. For instance, a bang-bang or sliding-mode control action can be achieved with appropriate settings, as illustrated in Fig. 12.

In another example, by setting r_3 to 0.008, a symmetrical sigmoid function is obtained, as shown in Fig. 13.

Consequently, the nonlinear controller φ has a wide range of control capabilities, exhibiting P-control, bang-bang control, and sliding-mode control action features with flexible switching between them.

Other control schemes considered in experimental studies are discrete PI and discrete SP-based PI controls to compare their performance with that of NPI.

The bilinear transformation (Tustin approach) is used for discrete-time PI control because it is a first-order approximation appropriate for low-order systems, and maps the left-hand plane (LHP) to points inside the unit circle while maintaining stability [24].

D. DISCRETE PI CONTROL LAW

The digital implementation of PI control in recursive form can be obtained by discretizing the integral term with the

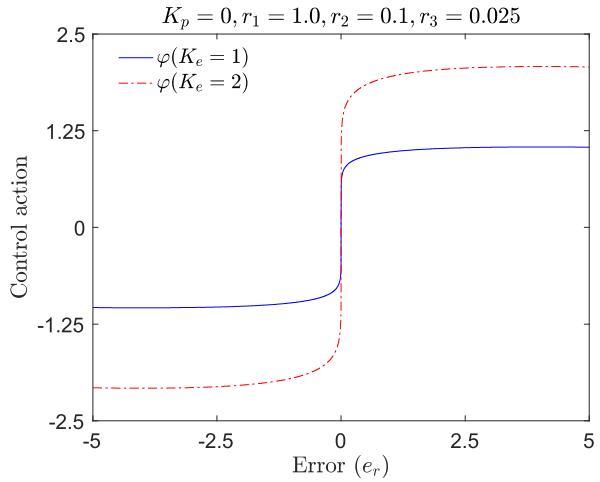

FIGURE 12. Abrupt change in control action.

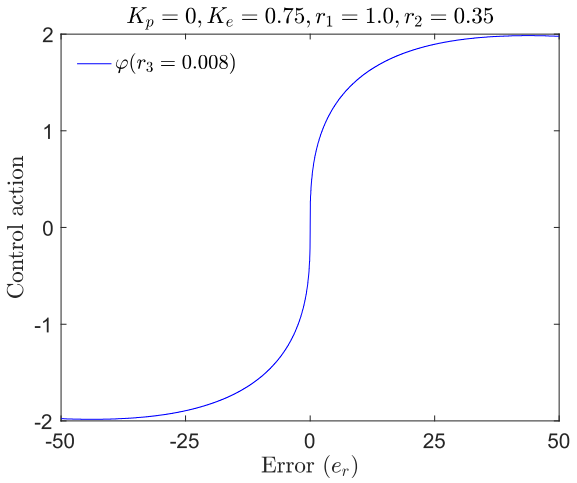

FIGURE 13. Symmetrical sigmoid control action.

sampling time T_s. Using the parallel form PI, the time- and frequency-domain representations of the control effort $u_{pi}(t)$ are given by

$$u_{pi}(t) = K_p e(t) + \frac{K_p}{\tau_i}\int_0^t e_r(\tau)\,d\tau \tag{7}$$

$$U_{pi}(s) = \left[K_p + \frac{K_i}{s}\right] E_r(s) \tag{8}$$

where $K_i = \frac{K_p}{\tau_i}$, τ_i is the integration time, K_p and K_i are the proportional and integral gain tuning parameters, respectively. By substituting the bilinear transformation [24] into (9), we obtain

$$U_{pi}(z) = \left[K_p + K_i\frac{T_s}{2}\frac{z+1}{z-1}\right] E_r(z) \tag{9}$$

rearranging (9), the control effort is represented in z-domain as

$$U_{pi}(z)(z-1) = \left[K_p(z-1) + \frac{K_i T_s}{2}(z+1)\right] E_r(z) \tag{10}$$

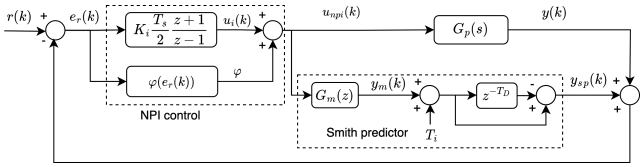

FIGURE 14. Plant schematic with NPI control and Smith predictor.

and in discrete form as

$$u_{pi}(k) = u_{pi}(k-1) + k_1 e_r(k) + k_2 e_r(k-1) \tag{11}$$

where $k_1 = K_p + \frac{K_i T_s}{2}$, $k_2 = -K_p + \frac{K_i T_s}{2}$. $u_{pi}(k)$ and $u_{pi}(k-1)$ are discrete-time related to the current and prior samples, respectively. Similarly, $e_r(k)$ and $e_r(k-1)$ are the current and previous discrete-time errors, respectively.

E. PLANT MODEL WITH DEADTIME

Plants with deadtimes mitigate the phase and gain margins [25], implying a lower damping ratio and a more oscillatory response. Such systems typically require predictive algorithms that estimate controlled variables to avoid unstable cases. In our case, a first-order plus time-delay plant model was developed using experimental data to allow the use of the Smith predictor, thus removing deadtime from the loop and boosting stability. An NPI control scheme was employed to improve the transient error and disturbance rejection effectively, as shown in Fig. 14.

In the above diagram, $r(k)$, $e_r(k)$, $u_i(k)$, φ, $u_{npi}(k)$, $y(k)$, $G_p(s)$, and T_i are the desired output, error signal, PI controller, nonlinear controller, NPI controller, controlled variable (temperature inside the incubator tank), dead-time plant transfer function, and initial incubator temperature, respectively. The Smith predictor includes the plant model $G_m(z)$ without deadtime, a delay block with deadtime constant T_D in discrete time, an initial incubator temperature T_i, and an SP output $y_{sp}(k)$. T_i is the initial incubator temperature, which was initially approximately the same as the ambient temperature, T_a. The initial temperature is measured only once using a microprocessor and is assigned a fixed value. Here, instead of setting the initial predictive temperature of the Smith predictor model to $0°C$, the actual incubator temperature was taken as the initial temperature T_i. Thus, the SP model can provide the predicted temperature more quickly using a more accurate initial temperature value.

III. RESULTS AND DISCUSSION

The experimental setup consisted of a microcontroller-based control and monitoring computer interface developed in C#, an incubator tank, and heating (150-W heater) and cooling (1-kW cooling fan) equipment, as shown in Fig. 2.

The computer user interface briefly enables the selection of controller type, controller setting parameters, and model parameters. It also makes it possible to enter the experimental start/stop times and disturbance injection time, visually

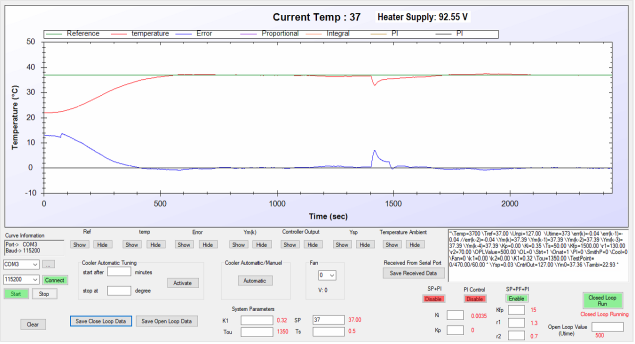

FIGURE 15. User interface screen and a scene from an experiment.

monitor the temperature, save data, and establish data communication with the microcontroller, as illustrated in Fig. 15.

Fig. 16 shows the experimental setup of the overall incubator control system.

The controller unit, shown in Fig. 17 (left), includes the ATMEGA 2560 kit, incubation test, and alarm circuit. It controls the equipment and communicates with the computer. The heating and cooling drives were connected to the incubator control card through I/O ports. The heating drive card in Fig. 17 (middle) consists of an AC switch driver (MOC3041) with an SCR-based switching element (TRIAC, BT139).

The cooling driver card in Fig. 17 (right) is identical to the heating drive; additionally, it has an isolated zero-cross detector and a temperature sensor circuitry.

The disturbance effect, rather than a complicated disturbance model, is considered a total undefinable constant temperature due to the lower temperatures at the initial location of the blood samples, ambient temperature, and open and closed durations of the incubator lid. Therefore, a cooling device was used to produce a constant disturbance effect during performance tests. It also increases the capacity for iterative experimentation by providing a quick return to initial conditions. A cooling fan, which causes a rapid temperature drop in the incubator tank, was employed to inject disturbances into the plant to determine the controller performance. In normal operation, the fan is not necessary and is therefore not included in the real system. By selecting a sampling time of $T_s = 0.5$ s, which is shorter than required, the incubator temperature is monitored precisely, and the sudden variations are logged accurately. Another reason is to rapidly show a graphical representation of sudden changes in incubator temperature. The display could not be refreshed quickly if the sampling time was set to several seconds. However, selecting a lower sampling time did not cause any numerical problems in the microprocessor, because double-precision calculations were used in the programming (code).

Fig. 18 shows the disturbance effect of the cooling fan, the rapid reduction in plant temperature, and the plant's natural behavior after disabling the controller and supply. The disturbance was injected into the plant while kept at $37°C$ and de-energized when the temperature drops to $33.2°C$.

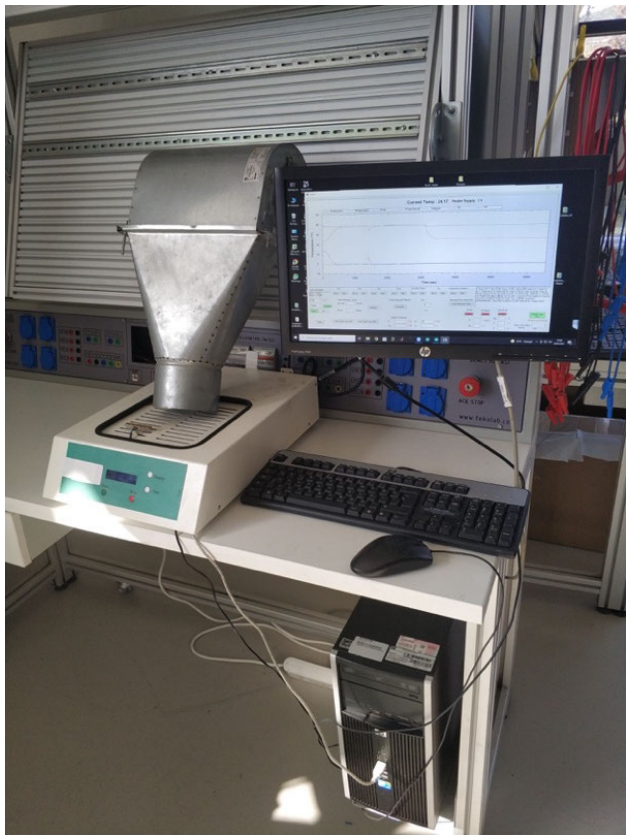

FIGURE 16. Experiment setup of incubator system.

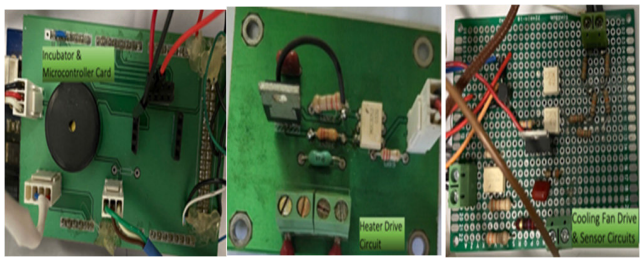

FIGURE 17. Control card and heater driving and cooling fan driver cards.

Meanwhile, the plant temperature resumes to decline and falls to a minimum temperature of $32.63°C$ due to the cooled air mass and inner walls inside the incubator. Then, the temperature starts to rise again at almost the same rate owing to heater inertia. After a certain amount of time, the temperature slope of the plant gradually decreases and eventually becomes negative.

Fig. 19 shows the temperature change over time in the incubator, left to free cooling with the heater off while the plant kept 37 $°C$ and ambient temperature was $T_a = 20.30°C$. Plant temperature exhibited exponential behavior, with an initial rapid drop of several degrees, followed by a steadily decreasing slope. Thus, a cooling fan is almost not required to reduce higher temperatures while the plant is maintained at body temperature ($37°C$). However, a cooling fan inside an incubator running throughout formal hours is not preferable

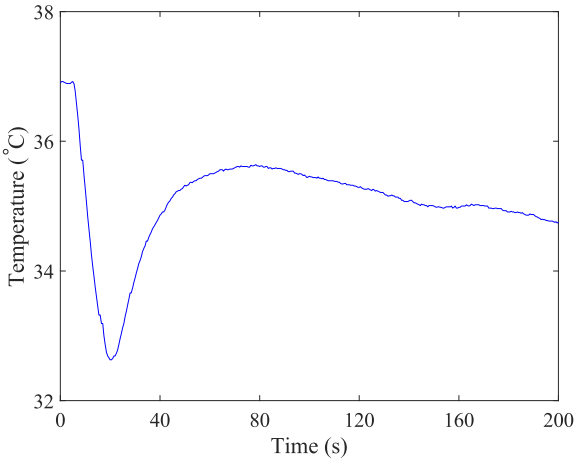

FIGURE 18. Plant's natural response to disturbance input.

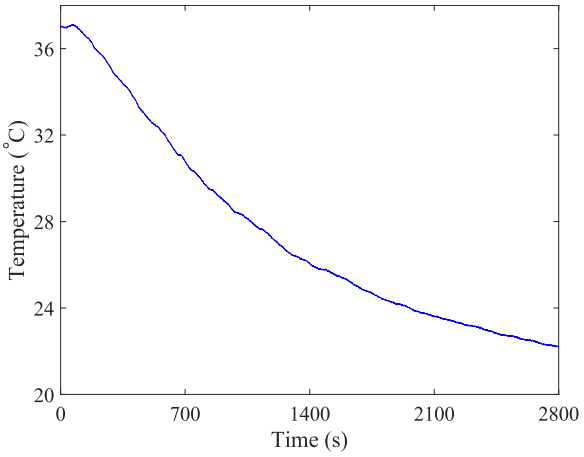

FIGURE 19. Leaving the incubator to cool.

for removing the excess heat. It loses its function or malfunctions over time because of its constant operation and dust collection.

A. CONTROL SIGNAL AND MAPPING

The lower and upper limits owing to the dead zone from the heater's thermal inertia and saturation and due to the peak regions of the sinusoidal supply voltage, respectively, were experimentally determined to correctly apply the control signal u_{npi} to the final control element (triac) via the driver. u_{npi} is converted into a gate-firing angle. The firing angle range was determined by dividing the half-cycle of the supply voltage (220 V AC, 50 Hz) into 500 slices using a 20-us interrupt timer, corresponding to 0-10 ms ($500 \times 20\ \mu$s) or 0-180 degrees interval. The firing angle range was then mapped to lower and upper limits of 70 and 470, respectively. Subsequently, the u_{npi} is arranged to be applied to the triac driver, as in (12), taking these limits into account.

$$u_t = 500 - int\left(u_{npi}\right) \tag{12}$$

where $int\left(u_{npi}\right) \leq 500$.

Finally, u_t is converted to the signal varying in a 0-10 ms interval, yielding the time-based firing angle t_α as in (13).

$$t_\alpha = \left(\frac{10}{500}\right) u_t \tag{13}$$

Timer1 in the embedded controller was initiated to determine t_α by using an external interrupt (RISING edge signal) produced by the zero-crossing detector at the zero-crossing instant of the supply voltage. Note that the Timer1 interrupt repeatedly calls the method firing_counter, developed in the embedded controller, every 20 us. When the counter variable in the method equals the firing angle t_α, the embedded controller sends a triggering signal to turn the triac on and simultaneously resets the counter variable to be ready for a new external interrupt. A small portion of the source code shows how to set external and timer interruptions.

```
attachInterrupt(2, zero_crossing_detect, RISING);
Timer1.initialize(freqStep); // freqStep = 20 us
Timer1.attachInterrupt(firing_counter, freqStep);
```

Fig. 20 illustrates the variation in the heater voltage (RMS) versus the firing angle obtained from the experimental data. Note that the control signal versus the heater (load) voltage exhibits a nonlinear relationship owing to the sinusoidal supply voltage. The firing angle time range is reduced to 3.5 ms to 9 ms (red circles) to provide a linear match with the corresponding load voltages, outside the saturation region, as shown in the figure.

A few experiments were carried out to determine the relationship between the supply voltage and time-based firing angle. Because of the nonlinear relationship, a fourth-order polynomial, as in (14), was built using a curve-fitting method.

$$V_{spp} = 5.88t_\alpha^4 + 2.65t_\alpha^3 - 45.26t_\alpha^2 - 74.79t_\alpha + 197.3. \tag{14}$$

B. HEATING MODELING

A temperature-varying system with time-delay dynamics can be modelled using three parameters, as shown in (15).

$$G(s) = \frac{Y(s)}{U(s)} = \frac{K}{1+\tau s} e^{-T_d s} \tag{15}$$

where τ, T_d, K, U, and Y are the process time constant, dead-time constant, static gain of the process, manipulated variable, and controlled (process) variable, respectively.

As shown in Fig. 21, the temperature dynamics data were collected every 0.5 s while implementing the open-loop step response by applying a supply voltage of 87 V.

As shown in the response curve, in addition to the dead time, the slope of the curve gradually decreased as the temperature increased. Accordingly, the FOPDT model describes the plant reasonably well. The response curve indicates that the deadtime T_d and time constant τ are 78 s and 1349 s, respectively, with the initial incubator temperature T_i =19.68°C.

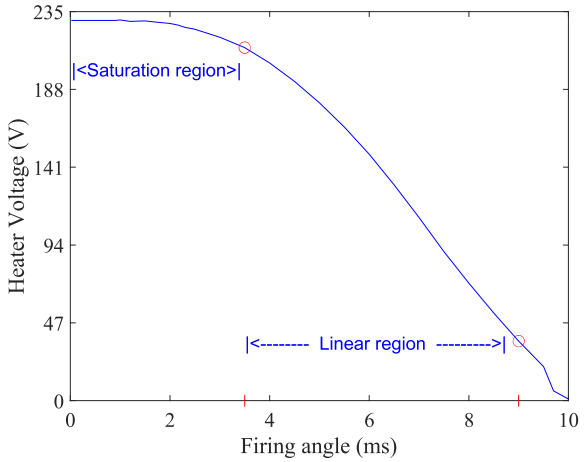

FIGURE 20. Phase voltage across the load (heater) vs firing angle.

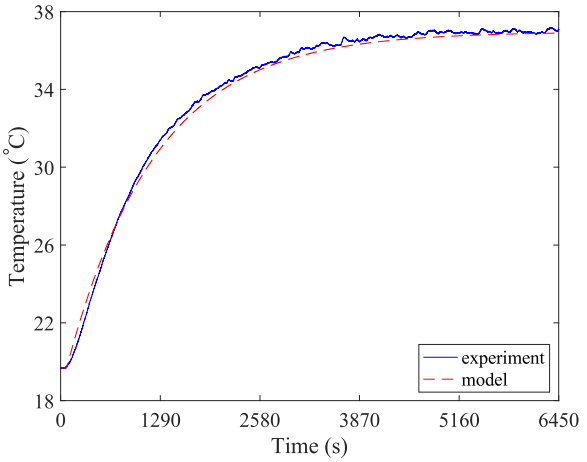

FIGURE 21. Measured and simulated model output.

The process or static gain K is introduced by the ratio, as in (16), of the incubator temperature (the controlled variable) to the input voltage (the manipulated variable) as follows:

$$K = \frac{\Delta y}{\Delta u} = \frac{T(\infty) - T_i}{u(t) - u(t_i)} = \frac{37 - 19.68}{87 - 34} = 0.32 \quad (16)$$

where $T(\infty)$, T_i, $u(t)$, and $u(t_i)$ represent the incubator temperature, initial temperature, input voltage, and initial (dead-zone) input voltage, respectively.

The incubator model parameters were calculated using MATLAB system identification toolbox. The simulation curve largely coincides with the measured data, as shown in Fig. 21. The plant model can be identified as a transfer function in the s-domain (17) and z-domain (18) by using a bilinear transform with $T_s = 0.5$s.

$$G_{md}(s) = \frac{K}{\tau s + 1} e^{-T_d s} = \frac{0.32}{1349s + 1} e^{-78s} \quad (17)$$

$$G_{mD}(z) = \frac{5.929x10^{-5}(z+1)}{z - 0.9996} z^{-156}. \quad (18)$$

G_m is chosen as a strictly proper function, as shown in (19), without deadtime to avoid an algebraic loop through the SP and controller.

$$G_m(z) = \frac{Y(z)}{U(z)} = \frac{5.929x10^{-5}(z+1)}{z(z - 0.9996)}. \quad (19)$$

Accordingly, the corresponding discrete-time sample delay T_D, as shown in Fig 14, was 155.

Another noteworthy point is that the deadtime to time constant ratio in (17) is low in the open-loop control implementation. In contrast, it effectively increases with closed-loop control and quality control schemes, as shown in the controller performance tests in Part C. Therefore, the controller faces a heavier delay problem, including plant nonlinearities. Thus, the SP is a part of the control structure.

The corresponding difference equation used in the source code to represent the plant model $G_m(z)$ is

$$y_m(k) = 0.9996y_m(k-1) + 5.929\times10^{-5}\left(u_{npi}(k-1) + u_{npi}(k-2)\right) \quad (20)$$

where $y_m(k)$ is the delay-free plant output and $u_{npi}(k)$ is the NPI control afford. Considering the SP block diagram in Fig. 14, the difference equation for the SP output (y_{sp}) can be expressed as:

$$y_{m\_T_i}(k) = y_m(k) + T_i \quad (21)$$

$$y_{sp}(k) = y_{m\_T_i}(k) - y_{m\_T_i}(k - T_D) \quad (22)$$

where $y_{m\_T_i}$ is the delay-free model output plus the incubator initial temperature.

C. PERFORMANCE TESTS

This section discusses the experimental results obtained from the performance tests in terms of transient response, steady-state response, and disturbance rejection. The model parameters τ, T_d, and K were assumed to remain unchanged throughout the performance tests, including the Ref (setpoint) and T_s. The controller output was limited to a range of 70 - 470, avoiding possible dead zones and saturation to improve the linearity of the dynamic response of the controller.

The following three incubator performance control tests addressed the fixed-setpoint control experiments. The test duration, including the disturbance, was continued until the end of the incubation period to assess performance differences between the control schemes. The cooling fan employed for the disturbance injection was disconnected when the temperature dropped to $33°C$ for each experiment. At each start, the ambient temperature T_a may differ slightly, whereas the initial temperature T_i in the incubator is almost the same, as shown in the figures. The first test was performed using a (PI) controller. The remaining control schemes use an SP as the dead-time compensator.

The PI control coefficients $K_p = 20$ and $K_i = 0.0015$, in Fig. 22 are fine-tuned to avoid oscillations. Due to the low-frequency damping, the incubator temperature (output) could not reach the setpoint within the required time, as shown in the figure. Quite long after the transient response, a disturbance was injected into the plant for 1400 s to assess the

controller's success. This causes the temperature to decrease to a minimum of $33°C$, as shown in the figure. The settling time (to Ref) takes 465 s from the activation moment of the disturbance. The output settles to the setpoint with a slightly high overshoot and a negligible steady-state error.

The temperature control with the SP-based PI control, as shown in Fig. 23, significantly outperformed the previous test with fine-tuned coefficients of $K_p = 25$ and $K_i = 0.0025$. The K_i is selected to be higher than the former coefficient owing to the eliminated dead-time effect.

The control effort produced higher outputs at start-up and disturbance injection to achieve faster settling times. Due to its predictive structure, SP prevents possible oscillations in the plant output.

The final test is implemented using the proposed (SP-based NPI) control, as shown in Fig. 24. To appropriately set the control action, the r_1 was set to 1.2, K_p to 20 to achieve a faster response, r_2 to 0.45 (the slope) for moderate nonlinearity, K_e to 30 for the required gain in the small-error region, and r_3 to 0.85, to keep the plant output stable in accordance with the preceding settings. The test results in the figure demonstrate the best performance in terms of transient response, settling time, disturbance rejection, and steady-state response. Due to its nonlinearity, the proposed controller significantly reduced the transient and disturbance settling times with a lower overshoot, although it used a higher value of K_i.

Table 1 lists the performance data for the fixed-setpoint implementations with disturbances. From measures such as overshoot (OS%), gain margin, phase margin, settling time, and steady-state error, the last two requirements were picked to determine the best control performance. A typical tolerance band of 2%, as listed in Tables 1 and 2, was employed as the settling time criterion in the tests to obtain performance data. Based on previous experience, the incubator temperature reached a steady state with the PI controller without a predictor in approximately 600 s. Accordingly, the steady-state errors (last column) were logged 600 s after the disturbance was injected, as shown in the table.

The table shows that NPI control outperforms the previous performance tests with significantly lower specification values. The proposed controller achieved a much faster response with the shortest transient and disturbance settling times.

For a more in-depth comparison, the steady-state error variations in the fixed-setpoint tests (beyond 1900 s) are illustrated in a single plot in Fig. 25. Note that the proposed control has much less oscillation and offset errors, and quickly reaches a steady state at approximately 1900 s.

The following setpoint tracking ($29°C$-$38°C$-$34°C$) tests attempt to measure and compare the controller performances with the well-tuned set parameters. As illustrated in Fig. 26, the PI control with well-tuned coefficients exhibited a lower performance at the lowest and highest abrupt change setpoints. Fortunately, it achieves a better performance when the temperature suddenly falls from the top setpoint to the middle.

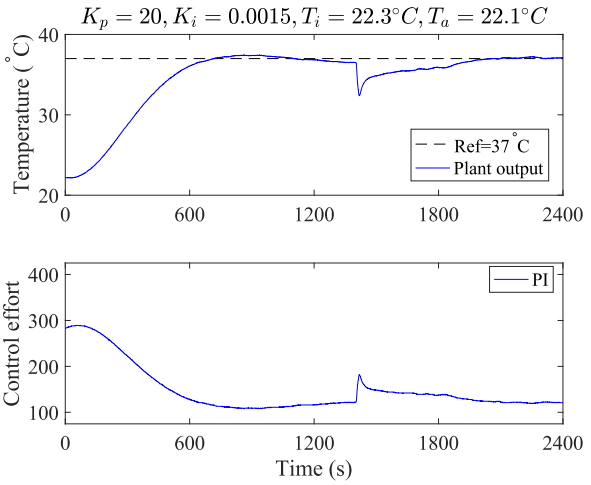

FIGURE 22. Performance test of PI control (PI).

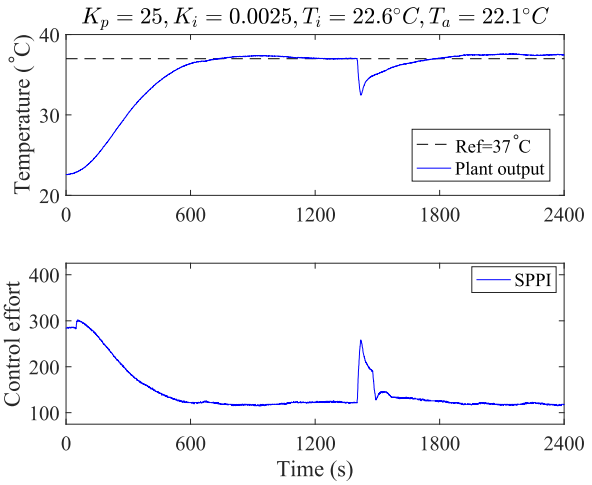

FIGURE 23. Performance test of SP-based PI control (SPPI).

Fig. 27 shows that the SP-based PI achieved better tracking than the PI with the set parameters. However, it exhibited the worst performance when a sudden temperature drop occurred from the highest setpoint ($38°C$), and still performed slightly better at the lower (middle) setpoint tracking. As shown in Fig. 28, the proposed (SP-based NPI) control with tuned parameters of $K_p = 18, K_i = 0.004, K_e = 25, r_1 = 1.20$, $r_2 = 0.80$ and $r_3 = 0.85$ accomplishes the best performance for each setpoint in terms of transient and steady-state responses with the lowest specification values. Unlike the others, when the setpoint is suddenly reduced to a sufficiently large extent, the control effort suddenly takes its minimum value (off) and stays at this value for a while; thus, the output settles to the setpoint faster with free cooling.

Table 2 lists the performance specification data for different abrupt change setpoints (Ref1, Ref2, and Ref3). The steady-state errors (last column) were logged 600 s after the third setpoint was activated, as listed in the table. Note that the steady-state error values are higher than those in

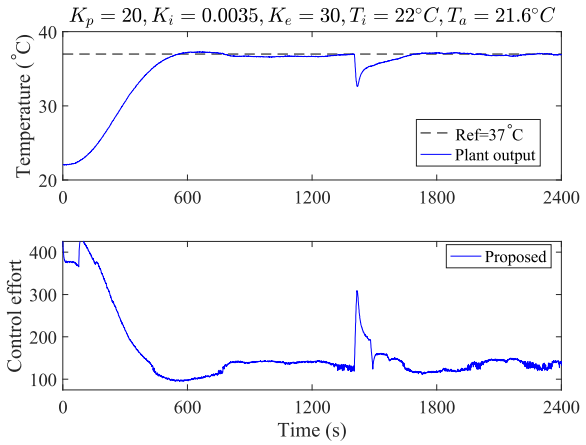

FIGURE 24. Performance test of proposed controller with tuning parameters of $r_1 = 1.2$, $r_2 = 0.45$, and $r_3 = 0.85$.

TABLE 1. Performance comparisons with fixed-setpoint.

Controller type	Transient settling time	Disturbance settling time	Steady-state error
	$t_s(s), 2\%$	$t_{ds}(s), 2\%$	$e_{rss}(°C)$
PI	620	325	0.15
SPPI	588	220	-0.44
Proposed	493	205	0.02

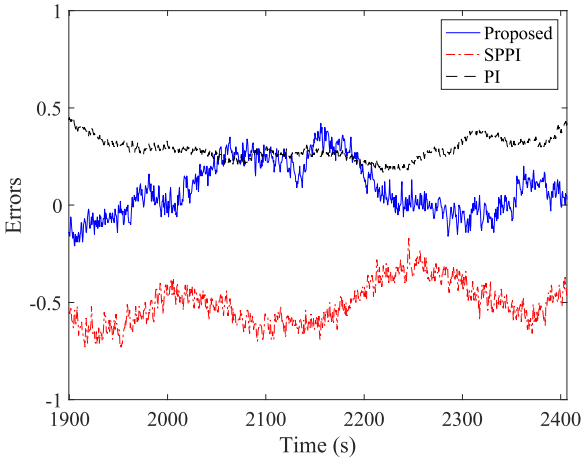

FIGURE 25. Steady-state errors.

Table 1, because the controller can lower the incubator temperature more slowly to a lower set point by freely cooling the incubator.

According to Table 2, the NPI control again achieves the lowest specification values compared to the others. It also exhibited significantly fewer oscillations at the highest set-point. On the other hand, the remaining controllers indicate lower performance, as they cannot settle the plant outputs down to the first set point by the 2% criterion, owing to higher overshoots.

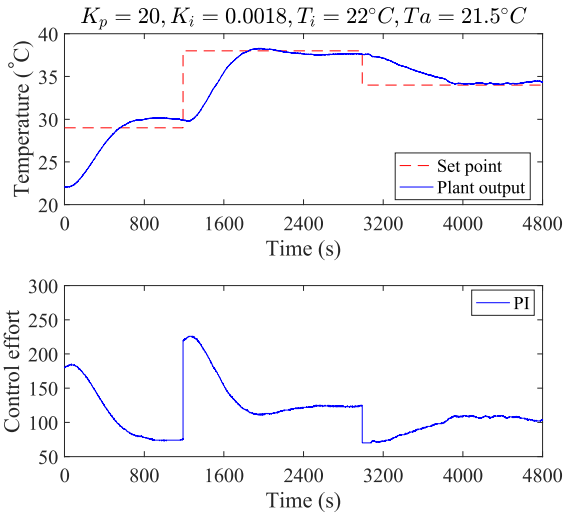

FIGURE 26. Set point tracking response for PI control with control effort.

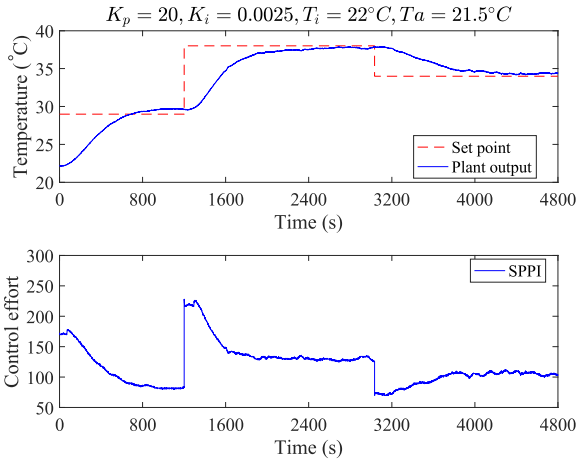

FIGURE 27. Set point tracking response for SP-based PI control with control effort.

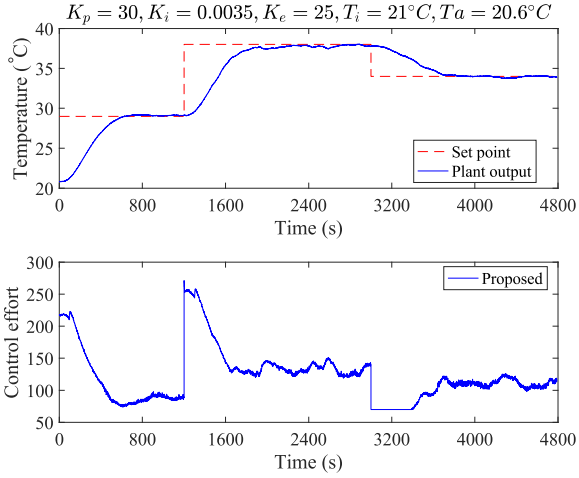

FIGURE 28. Set the point tracking response of the proposed control with tuning parameters of $r_1 = 1.2$, $r_2 = 0.80$, $r_3 = 0.85$ and control effort.

Consequently, the performances of the PI and SP-based PI (SPPI) controllers significantly decreased when tracking the

TABLE 2. Performance comparisons with abruptly changing setpoints.

Controller type	Transient settling time, $t_s(s)$, 2%			Steady-state error $e_{rss}(°C)$
	Ref1 ($29°C$)	Ref2 ($38°C$)	Ref3 ($34°C$)	
PI	not settled	547	830	1.63
SPPI	not settled	930	1035	1.12
Proposed	515	524	615	0.78

abrupt change setpoints, whereas the NPI performance was slightly affected.

IV. CONCLUSION

For blood grouping, the gel card incubator serves as a significant intermediate process, maintaining the gel cards at body temperature during incubation. Stabilizing the temperature and shortening the processing time are crucial for saving time and energy, because of the constant repetition of tasks. Therefore, a qualified control approach is required to reduce the warm-up phase with a shorter settling time and to avoid overshoot. Experimental results and literature reports [17] show that conventional schemes, such as PI- or SP-based PI, cannot achieve adequate performance in dead-time processes.

This study proposes a novel, readily tuned nonlinear plus integral controller accompanied by a dead-time compensator. The NPI control strategy provides a flexible and high-performance implementation by governing the linear and nonlinear control actions that enable soft transitions. That is, the controller can provide linear-to-nonlinear signals by adjusting its parameters.

The disturbance of the plant, rather than a complicated disturbance model, can be handled as a totally undefinable constant for the incubation process. This is mainly due to the lower temperatures at the initial location of the gel cards, ambient temperature, and the open and closed periods of the incubator lid. Therefore, a cooling device was employed for the experimentally proposed constant disturbance effect. It also helps to perform iterative experiments quickly by enabling a quick return to the initial conditions.

Comparative performance tests confirm the effectiveness and superiority of the proposed control strategy. For the fixed-setpoint test, the NPI reduced the transient response time by 20.48% and 16.16% compared with the PI and SP-based PI, respectively. Similarly, the NPI reduced the transient response time after injecting the disturbance by 36.92% and 6.82% compared with the PI and SP-based PI, respectively. The performance of the PI- and SP-based PI controllers dropped significantly in the experiments with abrupt change setpoints, although the performance of NPI was only slightly affected.

The test results show that when modifying the setpoint or injecting a disturbance into the incubator, the proposed nonlinear controller can effectively improve plant performance by regulating the incubator temperature more swiftly and accurately with minor steady-state errors and overshoots. Thus, the control quality was increased, reducing the warm-up phase and energy consumption. Furthermore, the gel card's temperature was appropriately brought to and maintained at body temperature to avoid deterioration of the blood sample due to overheating. In conclusion, the proposed NPI strategy efficiently improves the incubation performance and promises high potential to be employed in the industry owing to its readily tuned nonlinear structure and enables faster zero-error tracking control. Future research can focus on addressing problems with variable dead time and improving NPI controller parameters using nature-inspired algorithms such as bacterial foraging optimization (BFO), ant colony optimization (ACO), and particle swarm optimization (PSO).

REFERENCES

[1] A. Peci, A.-L. Winter, and J. B. Gubbay, "Evaluation and comparison of multiple test methods, including real-time PCR, for *Legionella* detection in clinical specimens," *Frontiers Public Health*, vol. 4, p. 175, Aug. 2016, doi: 10.3389/FPUBH.2016.00175.

[2] M. A. Zermani, "Application of adaptive predictive control to a newborn incubator," *Amer. J. Eng. Appl. Sci.*, vol. 4, no. 2, pp. 235–243, Feb. 2011.

[3] B. C. Torrico, M. U. Cavalcante, A. P. S. Braga, J. E. Normey-Rico, and A. A. M. Albuquerque, "Simple tuning rules for dead-time compensation of stable, integrative, and unstable first-order dead-time processes," *Ind. Eng. Chem. Res.*, vol. 52, no. 33, pp. 11646–11654, Jul. 2013.

[4] E. Spada, R. Perego, L. Baggiani, and D. Proverbio, "Comparison of conventional tube and gel-based agglutination tests for AB system blood typing in cat," *Frontiers Vet. Sci.*, vol. 7, p. 312, Jun. 2020.

[5] A. Roch, N. J. Magon, J. Maire, C. Suarna, A. Ayer, S. Waldvogel, B. A. Imhof, M. J. Koury, R. Stocker, and M. Schapira, "Transition to 37 °C reveals importance of NADPH in mitigating oxidative stress in stored RBCs," *JCI Insight*, vol. 4, no. 21, Nov. 2019, Art. no. e126376, doi: 10.1172/JCI.INSIGHT.126376.

[6] C. A. Manderson, H. McLiesh, R. Curvello, R. F. Tabor, J. Manolios, and G. Garnier, "Photothermal incubation of red blood cells by laser for rapid pre-transfusion blood group typing," *Sci. Rep.*, vol. 9, no. 1, p. 11221, Dec. 2019, doi: 10.1038/S41598-019-47646-Y.

[7] A. Visioli and Q.-C. Zhong, *Control of Integral Processes With Dead Time*. New York, NY, USA: Springer, 2011, pp. 233–239.

[8] M. Chèbre, Y. Creff, and N. Petit, "Feedback control and optimization for the production of commercial fuels by blending," *J. Process Control*, vol. 20, no. 4, pp. 441–451, Apr. 2010, doi: 10.1016/J.JPROCONT.2010.01.008.

[9] M. Jankovic and S. Magner, "Disturbance attenuation in time-delay systems—A case study on engine air-fuel ratio control," in *Proc. Amer. Control Conf.*, San Francisco, CA, USA, Jun. 2011, pp. 3326–3331.

[10] T. Maruyama, T. Shimura, A. Ejiri, Y. Ikai, and K. Shimotani, "Model predictive control applied to a diesel engine air-path system with dead time," in *Proc. SICE Annu. Conf.*, Tokyo, Japan, Sep. 2011, pp. 2628–2633.

[11] O. J. Smith, "Closed control of loop with dead time," *Chem. Eng. Prog.*, vol. 53, pp. 217–219, Jan. 1957.

[12] A. A. R. Coelho, R. Araujo, D. Jeronymo, and C. Suarez, "Discrete Smith predictor design and performance improvement of PID tuning," in *Proc. 11th IEEE/IAS Int. Conf. Ind. Appl.*, Dec. 2014, pp. 1–6.

[13] I. M. Iampita and S. B. Hisham, "Smith predictor-based controllers for temperature process with time delay," in *Proc. IEEE Student Conf. Res. Develop. (SCOReD)*, Oct. 2019, pp. 269–274, doi: 10.1109/SCORED.2019.8896245.

[14] A. H. Ahmadi and S. K. Y. Nikravesh, "Robust Smith predictor (RSP)," in *Proc. 24th Iranian Conf. Electr. Eng. (ICEE)*, May 2016, pp. 1510–1515.

[15] M. Huba, P. Bistak, T. Huba, and D. Vrancic, "Comparing filtered PID and Smith predictor control of a thermal plant," in *Proc. 19th Int. Conf. Electr. Drives Power Electron. (EDPE)*, Dubrovnik, Croatia, Oct. 2017, pp. 324–329.

[16] I. O. B. Gonzalez, R. R. Perez, V. F. Batlle, and F. J. C. Garcia, "Temperature control based on a modified Smith predictor for injectable drug formulations," *IEEE Latin Amer. Trans.*, vol. 13, no. 4, pp. 1041–1047, Apr. 2015.
[17] W. Xu, J. Zhang, and R. Zhang, "Application of multi-model switching predictive functional control on the temperature system of an electric heating furnace," *ISA Trans.*, vol. 68, pp. 287–292, May 2017.
[18] Y. Wang and Z. Liu, "Development of numerical modeling and temperature controller optimization for internal heating vacuum furnace," *IEEE Access*, vol. 9, pp. 126765–126773, 2021, doi: 10.1109/ACCESS.2021.3111319.
[19] P. Ele, J. B. Mbede, and E. Ondoua, "Parameters modelling and fuzzy control system of neonatal incubators," in *Proc. 5th Int. Conf., Sci. Electron., Technol. Inf. Telecommun.*, Mar. 2009, pp. 22–26.
[20] A. R. Shabaan, S. M. El-Metwally, M. M. Farghaly, and A. A. Sharawi, "PID and fuzzy logic optimized control for temperature in infant incubators," in *Proc. 5th Int. Conf. Modeling, Identificat. Control (ICMIC)*, vol. 2. Cairo, Egypt, Aug. 2013, pp. 53–59.
[21] S. B. Chen, L. Wu, and Q. L. Wang, "Self-learning fuzzy neural networks for control of uncertain systems with time delays," *IEEE Trans. Syst., Man, B, Cybern.*, vol. 27, no. 1, pp. 142–148, Feb. 1997, doi: 10.1109/3477.552196.
[22] G.-G. Jin and Y.-D. Son, "Design of a nonlinear PID controller and tuning rules for first-order plus time delay models," *Stud. Informat. Control*, vol. 28, no. 2, pp. 157–166, Jul. 2019.
[23] S. Yi, P. W. Nelson, and A. G. Ulsoy, "Proportional-integral control of first-order time-delay systems via eigenvalue assignment," *IEEE Trans. Control Syst. Technol.*, vol. 21, no. 5, pp. 1586–1594, Sep. 2013.
[24] Y. Jiang, X. Hu, and S. Wu, "Transformation matrix for time discretization based on Tustin's method," *Math. Problems Eng.*, vol. 2014, pp. 1–9, Jun. 2014.
[25] N. S. Özbek and İ. Eker, "Design of an optimal fractional fuzzy gain-scheduled Smith predictor for a time-delay process with experimental application," *ISA Trans.*, vol. 97, pp. 14–35, Feb. 2020, doi: 10.1016/J.ISATRA.2019.08.009.

M. ONAT (Member, IEEE) received the Ph.D. degree from Marmara University, Istanbul, Turkey, in 2001. He is currently an Associate Professor with the Electrical and Electronics Engineering Department, Faculty of Engineering, Marmara University.